Single-particle configurations of the excited states of ²⁰³Po

S. Chatterjee, B. Mondal, A. Ghosh, D. Arora, S. Das, S. Samanta, R. Raut, and S. S. Ghugre *UGC-DAE Consortium for Scientific Research, Kolkata Centre, Kolkata 700098, India*

P. C. Srivastava

Department of Physics, Indian Institute of Technology, Roorkee, Roorkee 247667, India

A. K. Sinha[®]

UGC-DAE Consortium for Scientific Research, University Campus, Khandwa Road, Indore 452017, India

U. Garg •

Department of Physics and Astronomy, University of Notre Dame, Notre Dame, Indiana 46556, USA

H. K. Singh 10

Department of Physics, Indian Institute of Technology, Bombay, Mumbai 400076, India

Neelam and K. Rojeeta Devi

Department of Physics and Astrophysics, University of Delhi, New Delhi 110007, India

A. Sharma 10

Department of Physics, Himachal Pradesh University, Shimla 171005, India

S. S. Bhattacharjee, R. Garg, I. Bala, R. P. Singh, and S. Muralithar *Inter University Accelerator Centre, New Delhi 110067, India*

(Received 2 August 2022; accepted 3 October 2022; published 31 October 2022)

Excited states of the 203 Po (Z=84, N=119) have been investigated after populating them through 194 Pt(13 C, 4 n) fusion-evaporation reaction at $E_{\rm beam}=74$ MeV and using a large array of Compton-suppressed HPGe clover detectors as the detection setup for the emitted γ rays. Standard techniques of γ -ray spectroscopy have been applied towards establishing the level structure of the nucleus. Twenty five new γ -ray transitions have been identified therein, through γ - γ coincidence measurements, and spin-parity assignments of several states have been determined or confirmed, following the angular correlation and linear polarization measurements on the observed γ rays. The excited states have been interpreted in the framework of large basis shell-model calculations, while comparing their calculated and experimental energies. They have been principally ascribed to proton population in the $h_{9/2}$ and $i_{13/2}$ orbitals outside the Z=82 closure and neutron occupation of the $f_{5/2}$, $p_{3/2}$, and $i_{13/2}$ orbitals in the N=126 shell.

DOI: 10.1103/PhysRevC.106.044329

I. INTRODUCTION

The shell model of the nucleus has remained its most credible microscopic description through more than seven decades now. Testing the model across the nuclear chart and refining the inputs, towards accomplishing better overlap with data, has been an agenda of nuclear structure studies through their evolving practice. The exercise is facilitated by developments in computational resources that help circumvent the dimensional challenges incurred in the application of the shell model, particularly to heavier systems such as those around Pb (Z=82). It may be noted that the very validity of the shell model for describing level structures around the proton Z=82 closure was a subject of early investigations in the

^{*}Present address: ONGC, Cinnamara Complex, Jorhat, Assam 785704, India.

 $^{^\}dagger Present$ address: Inter University Accelerator Centre, New Delhi 110067, India.

[‡]rajarshi.raut@gmail.com

[§]Present address: Department of Physics, Savitribai Phule Pune University, Pune, India.

[¶]Present address: Grand Accélérateur National d'Ions Lourds (GANIL), CEA/DRF-CNRS/IN2P3, BP 55027, 14076 Caen cedex 5, France.

region. While the closure at Z = 82 was identified to be sufficiently stable against collective excitations [1], it was also observed that light Hg (Z = 80) isotopes do exhibit collectivity and there were predictions of similar phenomena in the proton-rich side of the (Z = 82) closure, for the light Po (Z = 84) nuclei [2]. The studies undertaken towards resolving the proposition, however, froze on describing the excitations of light-Po isotopes, such as ^{199–201}Po, within the framework of the shell model. This was also commensurate with the systematically calculated [2] shapes of the Pb isotopes starting from 208 Pb (Z = 82, N = 126) and extending to the lighter ones. Doubly magic ²⁰⁸Pb, quite expectedly, exhibited deep energy minimum for a spherical shape; the minimum became shallower for lighter systems in the isotopic chain and eventually evolved into a double minima corresponding to both prolate and oblate deformations for nuclei as light as 190 Pb (Z=82, N=108). Such a scenario, however, was not established in 198 Pb or 202 Pb that still manifested near spherical shapes and it was found valid to interpret the excitation schemes of the neighboring light Po isotopes from the perspectives of the shell model. The merits of such interpretation notwithstanding, it was largely extracted from the evolution of experimentally observed level energies and their spacings across the isotopic and/or the isotonic chains. That was presumably owing to the limited wherewithal then available for computational endeavors but, nevertheless, could provide insights into the particle excitations underlying the level scheme of the nuclei being studied. The experimental findings in these studies mostly followed population of the nuclei of interest in α - or heavy-ion-induced fusion-evaporation reactions and detection of the γ rays using modest setups of a few Ge detectors and, at times, using conversion electron measurements.

The only existing precedence of spectroscopic study of the 203 Po (Z = 84, N = 119) nucleus, following its population in a fusion-evaporation reaction, was by Fant et al. [3]. The nucleus was populated using α -induced reaction on 204 Pb and the deexcitation γ rays were detected using small planar Ge(Li) detectors, large coaxial Ge(Li) detectors and intrinsic Ge detectors. Conversion electrons were also measured in conjunction. The level scheme of the nucleus was established up to an excitation energy of ≈4.4 MeV and spin \approx 18 \hbar . However, only a selected number of γ -ray transitions, presumably the strongest ones, and levels were identified above the 25/2⁺ state; the spin-parity assignments were considerably tentative therein. The configurations of the excited states were largely ascribed to the coupling of an odd neutron hole to the excitations of the even 204 Po-core (Z = 84, N = 120). Two configurations, based on proton excitations outside the closed proton shell of the ²⁰⁸Pb core, were identified in the latter. These were $\pi h_{9/2}^2$ and $\pi h_{9/2} i_{13/2}$ that resulted in maximum spins 8 and 11, respectively. The available single-particle orbitals for the odd neutron are $2f_{7/2}$, $1h_{9/2}$, $1i_{13/2}$, $3p_{3/2}$, $2f_{5/2}$, $3p_{1/2}$ and the first $5/2^-$, $3/2^-$, $1/2^-$, $13/2^+$ states in 203 Po were identified with single-neutron excitations therein. The $17/2^+$, $21/2^+$, and 25/2+ yrast states in odd-A Po isotopes were attributed to the odd neutron hole $vi_{13/2}^{-1}$ coupled to the excitations of the

corresponding Pb core or of the two valence protons of the Po core, resulting in states 2^+-8^+ . This followed the systematics of the yrast states in odd-A Pb and Po isotones. It may be noted that the yrast $17/2^+$ and the $21/2^+$ states in isotopes ¹⁹⁹⁻²⁰⁵Pb had been ascribed to pure neutron excitations, such as $\nu p_{1/2}^{-1} f_{5/2}^{-1} i_{13/2}^{-1}$ and $\nu f_{5/2}^{-2} i_{13/2}^{-1}$. However, such (pure neutron) excitations would result in states of higher excitation energies than those of the yrast $17/2^+$ and the $21/2^+$ levels in odd-A Po isotopes. It was thus found reasonable to assign the pure neutron excitations to the respective nonyrast states. The 27/2⁺ and the 29/2⁺ levels in the odd Po nuclei were identified with three-quasiparticle configurations $\pi h_{9/2}^2 \otimes \nu i_{13/2}^{-1}$. The configurations for the isomeric $25/2^-$ and $29/2^-$ were derived from their overlap with the systematics of these states observed in the Pb isotopes. Accordingly, their configuration in ²⁰³Po was identified to be similar to that in ²⁰¹Pb and the same is $(\pi(h_{9/2}^2)_{0^+}\otimes \nu p_{1/2}^{-2}f_{5/2}^{-3}(i_{13/2}^{-2})_{12^+})_{25/2^-29/2^-}$. The findings in ²⁰³Po thus upheld the interpretation of its excitation scheme within the framework of the single-particle excitations, as had been established for the still lighter isotopes of the nucleus [2]. This was also a continuing trend from the heavier isotopes such as ^{205,207}Po [1]. The absence of collectivity was further corroborated by the absence of enhanced B(E2) in these nuclei [3].

The present paper reports a spectroscopic investigation of the level structure of 203 Po, using the updated experimental facilities as well as contemporary framework for the shell-model calculations. The objective was to explore possible features in the excitation scheme of the nucleus, through the use of a large array of high-resolution γ -ray detectors in the setup, and to test the reproducibility of the observed level energies in the calculations carried out within the shell-model framework. The computational exercise is a validation of the model Hamiltonian used for the purpose as well as of facility in identifying and quantifying the single-particle excitations that contribute to the observed level scheme.

II. EXPERIMENTAL DETAILS AND DATA ANALYSIS

Excitations of the 203 Po nucleus were investigated following its population in the 194 Pt(13 C, 4 n) reaction at $E_{lab} =$ 74 MeV. The target was 13 mg/cm² thick self-supporting foil of enriched (99%) ¹⁹⁴Pt. The beam was delivered by the 15 UD Pelletron at IUAC, New Delhi and the beam energy was so chosen after an excitation function measurement at the commencement of the experiment. As per the predictions of the statistical model calculations, at this beam energy, the aforementioned reaction would be of dominant cross section among the possible compound nucleus fusionevaporation channels while the fission (exit) channel would amount to \approx 25% of the total fusion cross section. Indeed, the yield of ²⁰³Po was observed to be maximum when compared with the other fusion-evaporation products, which principally included isotopes of Po (Z = 84), Bi (Z = 83), and Pb (Z =82), as illustrated in Fig. 1. The detection system used was the Indian National Gamma Array (INGA) setup at IUAC [4] and (then) consisted of eighteen Compton suppressed HPGe clover detectors positioned at 148° (four detectors),

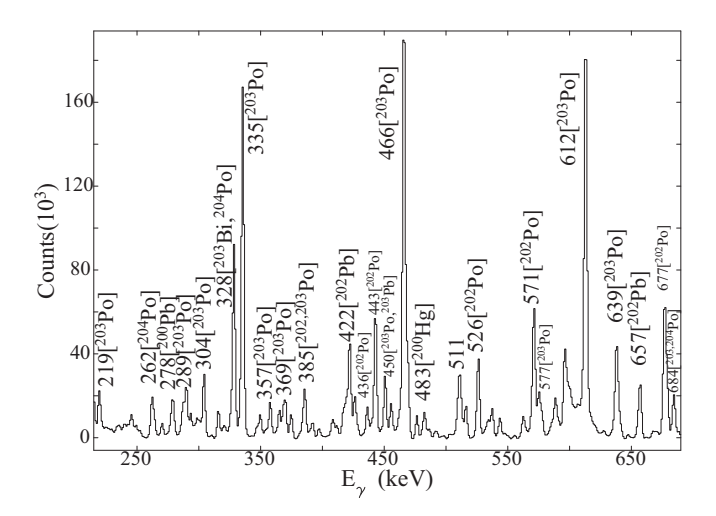


FIG. 1. Part of the γ -ray spectrum corresponding to the full projection of a γ - γ symmetric matrix and illustrating the different product nuclei populated in the present experiment.

 123° (four detectors), 90° (six detectors), 57° (two detectors), and 32° (two detectors). An assembly of three absorber sheets of lead, tin, and copper was fixed on the face of the hevimet collimator of the anti-Compton shield (ACS) in each detector. The absorbers facilitated in reducing the intensity of the x rays, from the thick target, being incident on the detectors (and thus contributing in the event trigger). Data were principally acquired under the condition that at least two Compton-suppressed HPGe clover detectors needed to fire in coincidence for generating the event trigger. The number of two- and higher-fold events acquired was $\approx 2 \times 10^9$.

The data were sorted into spectra, symmetric and asymmetric (angle dependent) $\gamma - \gamma$ matrices as well as a $\gamma - \gamma - \gamma$ cube using the SPRINGZ [5] code. The sorted data were subsequently analyzed using different routines of the RADWARE [6] package. The methodology and the objectives of the exercise were identical to that of any regular investigation of nuclear level structure using γ -ray spectroscopy. These have been detailed in numerous papers, such as Refs. [7,8], and are briefly mentioned herein. The coincidence relationships between the observed γ -ray transitions were extracted from the symmetric $\gamma - \gamma$ matrix and $\gamma - \gamma - \gamma$ cube. The coincidences along with the intensity considerations were applied for the placement of the γ -ray transitions in the level scheme of the nucleus. The assignment of multipolarities of the γ rays followed determination of their $R_{\rm ADO}$ (ratio of angular distribution from oriented nuclei) values using

$$R_{\rm ADO} = \frac{I_{\gamma 1} \text{ at } 32^{\circ} \text{ (Gated by } \gamma_2 \text{ at all angles)}}{I_{\gamma 1} \text{ at } 123^{\circ} \text{ (Gated by } \gamma_2 \text{ at all angles)}},$$
 (1)

where I is the intensity of the transition (of interest) γ_1 in the above equation in the relevant gated spectrum that is generated from the appropriate angle-dependent matrix. As far as this analysis is concerned, the $R_{\rm ADO}$ value for the stretched dipole ($\Delta J=1$) transitions is 0.73 ± 0.01 while for the stretched quadrupole ($\Delta J=2$) ones, it is 1.34 ± 0.01 . These values were derived from $R_{\rm ADO}$ of transitions with previously established multipolarities and belonging to other Po

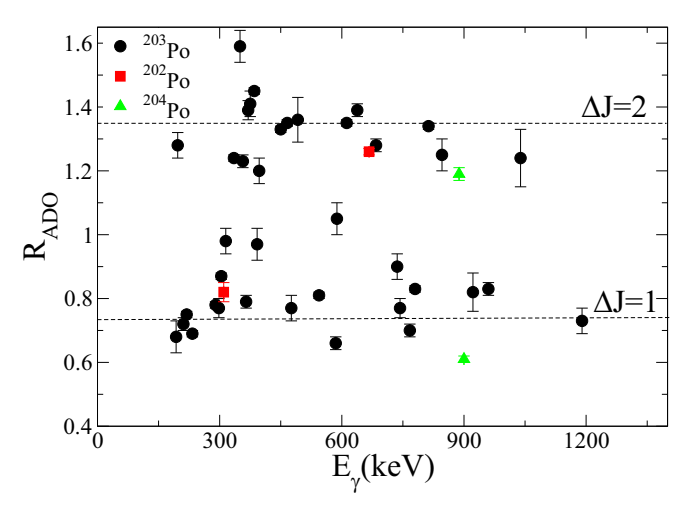


FIG. 2. $R_{\rm ADO}$ values for transitions of $^{203}{\rm Po}$, as determined in the current analysis. Those for selected transitions of $^{202,204}{\rm Po}$ are plotted as reference.

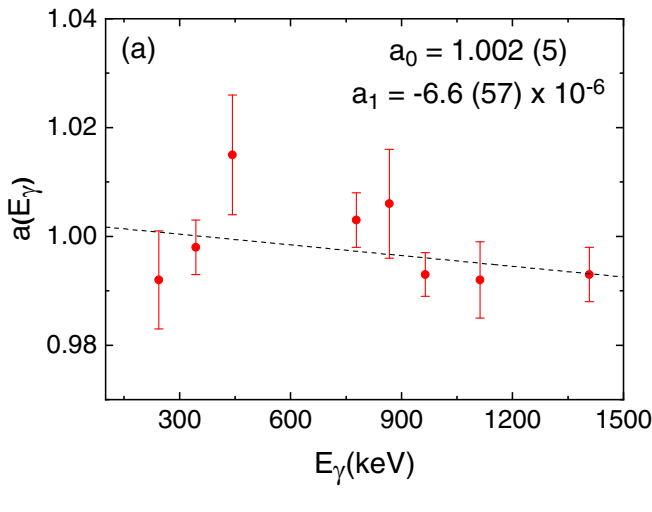
isotopes populated in the same experiment. The $R_{\rm ADO}$ values determined for different γ -ray transitions, observed in this study, are represented in Fig. 2.

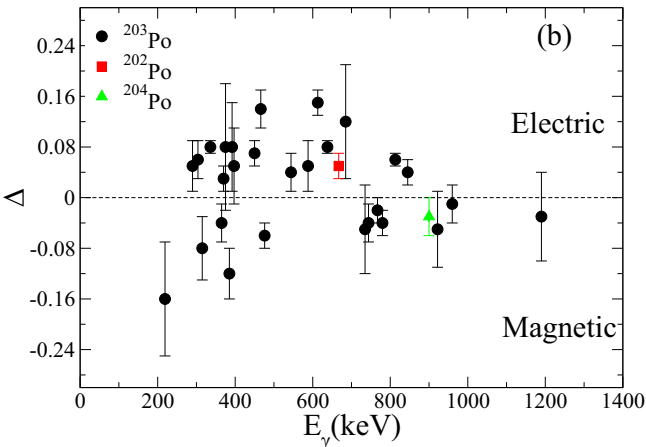
The electromagnetic nature of the transitions were assigned on the basis of their polarization asymmetry evaluated using

$$\Delta = \frac{aN_{\perp} - N_{\parallel}}{aN_{\perp} + N_{\parallel}},\tag{2}$$

where N_{\perp} and N_{\parallel} are respectively the number of photons of the γ rays of interest that are scattered perpendicular to and parallel to the reference plane. The latter is defined by the beam direction and the direction of emission of the γ ray. Each of the four crystals of a HPGe clover detector operates as scatterer while the two adjacent ones, parallel and perpendicular to the scatterer, operate as absorbers and facilitate the identification of the scattering events in the respective directions. The asymmetry between the two scattering possibilities is known to be maximum at 90°. Thus, the N_{\perp} (N_{\parallel}) for γ rays is extracted from a matrix that has been constructed with the perpendicular (parallel) scattering events in the detectors at 90° on one axis and the coincident detections in detectors at all other angles on the other axis. The coincidences aid in the unambiguous identification of the γ -ray transition being analyzed. The a in Eq. (2) represents the asymmetry that is characteristic to the geometry of the detection setup. It was determined from the asymmetry between N_{\perp} and N_{\parallel} for γ rays of (unpolarized) radioactive sources, such as ¹⁵²Eu, and using $a = N_{\parallel}/N_{\perp}$. The typical plot of a, as a function of γ -ray energy, for the present setup is illustrated in Fig. 3(a). The polarization asymmetry $[\Delta, as defined by Eq. (2)]$ values of the transitions of ²⁰³Po are plotted in Fig. 3(b). The observed asymmetry between N_{\perp} and N_{\parallel} for polarized γ rays, such as those emitted by spin oriented ensemble of nuclei produced in fusion-evaporation reactions, depends on the degree of their polarization P and the sensitivity Q of the measurement setup. These are related through

$$P = \frac{\Delta}{O},\tag{3}$$





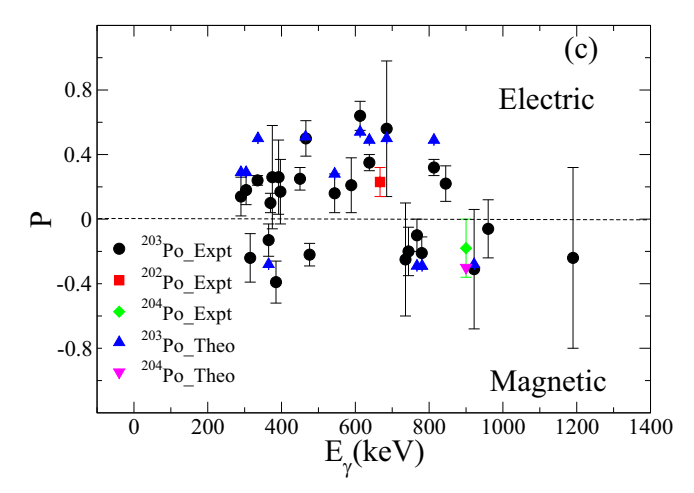


FIG. 3. (a) Plot of geometrical asymmetry as a function of γ -ray energy. (b) Polarization asymmetry of transitions of 203 Po. (c) Linear polarization values for transitions of 203 Po along with the corresponding theoretical estimates for some of them (of pure multipolarity). The Δ and P values for selected transitions of other isotopes, which were populated in the same experiment, are included for validation.

with

$$Q(E_{\gamma}) = Q_0(E_{\gamma})(CE_{\gamma} + D),$$
 (4)

where

$$Q_0(E_\gamma) = \frac{\alpha + 1}{\alpha^2 + \alpha + 1},\tag{5}$$

 α being E_{γ}/m_ec^2 , m_ec^2 is the electron rest mass energy. The *C* and *D* parameters for the purpose were adopted from those following the work by Palit *et al.* [9] and are $C = 0.000\,099 \text{ keV}^{-1}$ and D = 0.446. Figure 3(c) illustrates the plot of the *P* values determined for different transitions of ^{203}Po .

As per the regular methodology of nuclear structure studies, using γ -ray spectroscopy, the information on coincidence relationships between the γ rays along with their intensities, multipolarities, and electromagnetic nature, as resulting from the aforementioned analysis, were used to identify the excitation scheme of the nucleus and the same is discussed in the next section.

III. RESULTS

The excitation scheme of 203 Po, as established or confirmed in the present investigation, is illustrated in Fig. 4. Figures 5 and 6 illustrate the representative gated spectra respectively projected from γ - γ matrix and γ - γ - γ cube. The observed coincidences have been used to identify the placement of transitions in the level scheme. Twenty five new γ -ray transitions have been placed in the level scheme of the nucleus and the following modifications have been made in the existing [3,10] assignments therein. The details of the γ -ray transitions are recorded in Table I. (The energies of the transitions and the levels are rounded off to the nearest integer in the discussions herein.)

- (1) The placement of 397-keV transition has been changed with respect to that assigned in the literature, as deexciting a \approx 1527-keV level [11]. The level and the γ ray was not reported by Fant *et al.* while in the present study the placement of the transition has been modified to one deexciting the \approx 3264-keV state. The level has been marked as a new one in the level scheme (Fig. 4) while the γ -ray transition is identified to have been observed previously, albeit with a different placement.
- (2) The 219-keV transition deexciting the 2274-keV level has been identified as a *M*1 and the state has been identified to be of spin-parity 27/2⁺. There was no spin-parity assignment for this level, identified as ≈2277 keV by Fant *et al.* [10], in the previous studies.
- (3) The 959-keV transition, deexciting the 3014-keV state, has been tentatively assigned an (M)1 nature, following the present measurements. Accordingly, the state has been assigned a spin-parity of $27/2^{(+)}$ that is at variance with the assignment by Fant *et al.* [10]. The latter had identified the γ ray as a pure E2 one and had tentatively assigned the spin-parity of the state (≈ 3018 keV, as per Fant *et al.*) as $(29/2^+)$.
- (4) The 543-keV γ ray, from the 3066-keV state, has been assigned a multipolarity of E1 in this study. It was tentatively identified as M1, by Fant et al., and the spin of the level (at \approx 3070 keV, as per Fant et al.) was accordingly assigned to be 29/2.

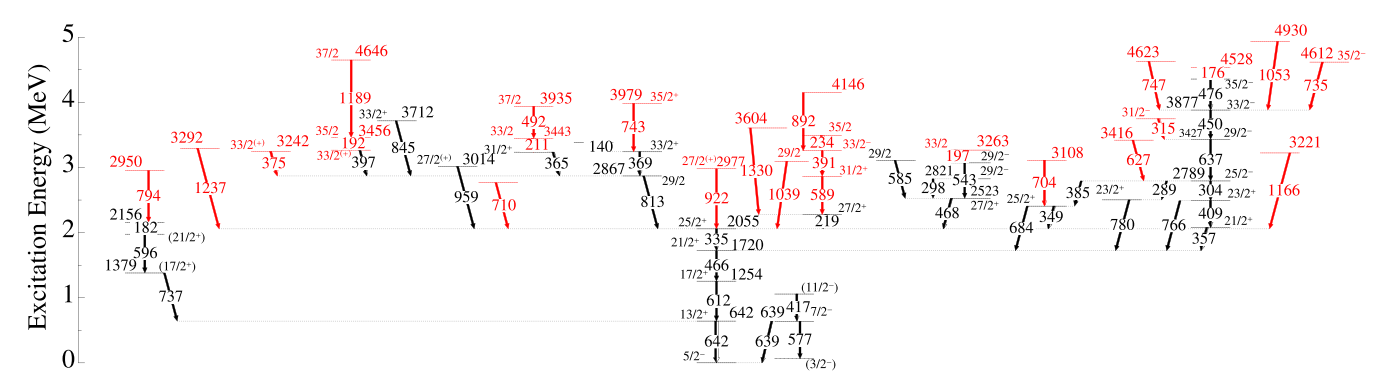
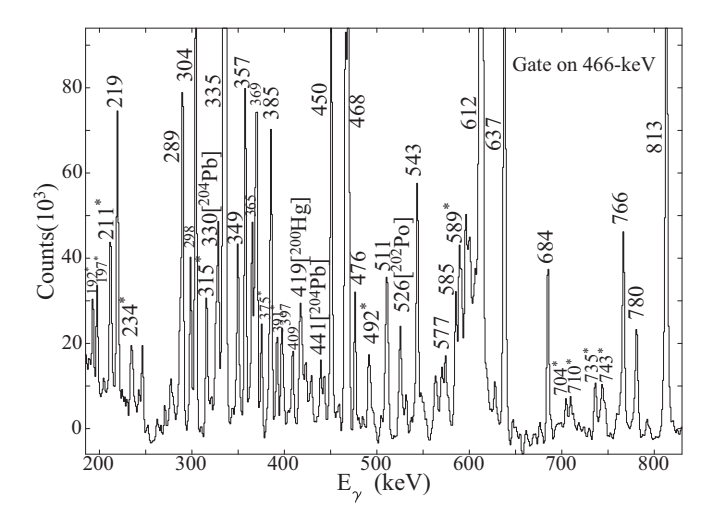


FIG. 4. Excitation scheme of 203 Po. The γ -ray transitions and the energy levels that have been newly identified in this study are indicated in red. The corresponding energy values are also indicated in red. The level energies, rounded off to the nearest integer, are mentioned for most (not all) of the states.

(5) The 585-keV transition deexciting the 3108-keV state has been established as a pure dipole in this study. However, the electromagnetic nature of the same could



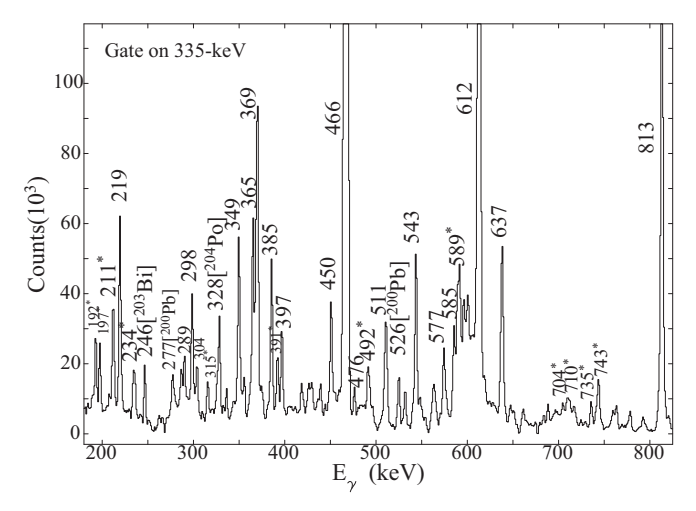


FIG. 5. Representative spectra projected out of γ - γ matrix with gate on transitions of ²⁰³Po, as indicated in the inset of the respective spectrum. The γ rays newly identified in the present work are marked with *. Those resulting from overlapping coincidences in other nuclei, populated in the same experiment, are also labeled accordingly.

- not be unambiguously determined in the present investigation. The multipolarity of the transition was undetermined in the work by Fant et~al. and consequently there was no spin assignment for the state (at $\approx 3112~\text{keV}$, as quoted by Fant et~al.) therein.
- (6) The spin-parity of the 3236-keV state, deexcited by the 369-keV transition, has been confirmed to be $33/2^+$ in this study. The assignment for the level (at \approx 3241 keV, as per Fant *et al.*) was only tentative in the previous work [10].
- (7) The spin-parity of the 3712-keV level has been assigned as $33/2^+$ in this work, following the E2 assignment of the 845-keV γ ray that deexcites the state. There was no multipolarity assignment for the transition or spin-parity assignment for the state (at \approx 3717 keV, as per Fant *et al.*) in the previous studies [10].
- (8) The 3877-keV state has been assigned spin-parity of 33/2⁻, in this measurement. This is following the identification of the 450-keV transition, that deexcites

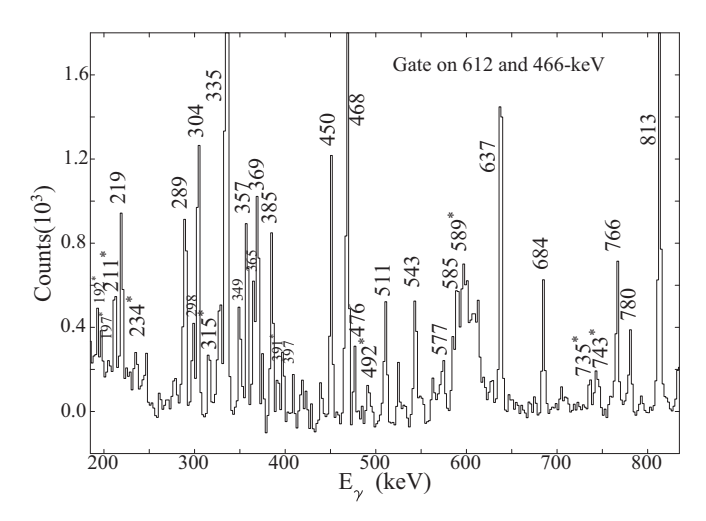


FIG. 6. Representative spectrum projected out of γ - γ - γ cube with double gate on transitions of ²⁰³Po, as indicated in the inset of the spectrum. The γ rays newly identified in the present work are marked with *.

TABLE I. Details of the levels and the γ -ray transitions of 203 Po nucleus observed in the present work. The energy of a γ -ray transition is the weighted average of its value in multiple gates. The relative intensities I_{γ} of the γ -ray transitions are normalized with respect to the intensity of 466-keV transition as observed in 612-keV gated spectrum. The ADO ratios $R_{\rm ADO}$, polarization asymmetry $\Delta_{\rm pol}$, and linear polarization P of the transitions are determined by using the procedure described in Sec. II. The D and Q in the column for multipolarity respectively represents dipole and quadrupole transitions; the polarization measurement could not be carried out for these transitions and thus their electromagnetic nature remains unassigned. The N superscript indicates the assignments that have been adopted from the data evaluation of A=203 nuclei by Kondev [10].

E_i (keV)	E_{γ} (keV)	E_f (keV)	I_{γ}	$oldsymbol{J}_i^\pi$	J_f^π	$R_{ m ADO}$	$\Delta_{ m pol}$	P	Multipolarity
638.7 ± 0.1	577.2 ± 0.1	61.5	11 ± 1	7/2-	(3/2-)				$E2^N$
	638.7 ± 0.1	0.0	48 ± 1	$7/2^{-}$	$5/2^{-}$				$M1^N$
641.7 ± 0.2	641.7 ± 0.2	0.0		$13/2^{+}$	$5/2^{-}$				$M4^N$
1055.2 ± 0.1	416.5 ± 0.1	638.7	59 ± 1	$(11/2^{-})$	$7/2^{-}$				$E2^N$
1254.0 ± 0.2	612.3 ± 0.1	641.7		$17/2^{+}$	$13/2^{+}$	1.35 ± 0.01	0.15 ± 0.02	0.64 ± 0.09	E2
1378.8 ± 0.3	737.1 ± 0.2	641.7	127 ± 3	$(17/2^+)$	$13/2^{+}$				$(E2)^N$
1719.8 ± 0.2	465.8 ± 0.1	1254.0	1000	$21/2^{+}$	$17/2^{+}$	1.35 ± 0.01	0.14 ± 0.03	0.50 ± 0.11	E2
1974.5 ± 0.3	595.7 ± 0.1	1378.8	118 ± 3	$(21/2^+)$	$(17/2^+)$				$E2^N$
2054.7 ± 0.2	334.9 ± 0.1	1719.8	643 ± 14	$25/2^{+}$	$21/2^{+}$	1.24 ± 0.01	0.08 ± 0.01	0.24 ± 0.03	E2
2077.0 ± 0.2	356.8 ± 0.1	1719.8	64 ± 2	$21/2^{+}$	$21/2^{+}$	1.23 ± 0.02			$M1^N$
2156.4 ± 0.3	181.9 ± 0.1	1974.5	75 ± 2		$(21/2^+)$				
2273.6 ± 0.2	219.1 ± 0.1	2054.7	58 ± 1	$27/2^{+}$	$25/2^{+}$	0.75 ± 0.01	-0.16 ± 0.09	-0.43 ± 0.24	M1
2404.2 ± 0.2	349.2 ± 0.1	2054.7	36 ± 1	$25/2^{+}$	$25/2^{+}$	1.59 ± 0.05			$M1^N$
	684.1 ± 0.1	1719.8	71 ± 2	$25/2^{+}$	$21/2^{+}$	1.28 ± 0.02	0.12 ± 0.09	0.56 ± 0.42	E2
2485.8 ± 0.2	408.6 ± 0.2	2077.0	21 ± 1	$23/2^{+}$	$21/2^{+}$				$M1^N$
	765.9 ± 0.1	1719.8	76 ± 2	$23/2^{+}$	$21/2^{+}$	0.70 ± 0.02	-0.02 ± 0.02	-0.10 ± 0.10	M1
2500.2 ± 0.2	780.1 ± 0.1	1719.8	40 ± 1	$23/2^{+}$	$21/2^{+}$	0.83 ± 0.01	-0.04 ± 0.02	-0.21 ± 0.10	<i>M</i> 1
2523.0 ± 0.2	468.3 ± 0.1	2054.7	176 ± 4	$27/2^{+}$	$25/2^{+}$				$M1^N$
2765.1 ± 0.4	710.4 ± 0.3	2054.7	8 ± 1	,	$25/2^{+}$				
2789.1 ± 0.2	289.3 ± 0.1	2500.2	35 ± 1	$25/2^{-}$	$23/2^{+}$	0.78 ± 0.01	0.05 ± 0.04	0.14 ± 0.12	E1
	303.5 ± 0.1	2485.8	102 ± 2	$25/2^{-}$	$23/2^{+}$	0.87 ± 0.01	0.06 ± 0.03	0.18 ± 0.09	E1
	385.1 ± 0.1	2404.2	54 ± 2	$25/2^{-}$	$25/2^{+}$	1.45 ± 0.01	-0.12 ± 0.04	-0.39 ± 0.13	$E1^{\mathbf{a}}$
2820.9 ± 0.2	297.7 ± 0.1	2523.0	28 ± 1	$29/2^{-}$	$27/2^{+}$	0.77 ± 0.03			$(E1)^N$
2863.0 ± 0.2	589.4 ± 0.1	2273.6	55 ± 2	$31/2^{+}$	27/2+	1.05 ± 0.05	0.05 ± 0.04	0.21 ± 0.17	E2(+M3)
2867.2 ± 0.2	812.5 ± 0.1	2054.7	226 ± 5	29/2+	25/2+	1.34 ± 0.01	0.06 ± 0.01	0.32 ± 0.05	E2
2950.0 ± 0.4	793.6 ± 0.2	2156.4	4 ± 1	,	,				
2976.7 ± 0.3	922.2 ± 0.2	2054.7	13 ± 1	$27/2^{(+)}$	$25/2^{+}$	0.82 ± 0.06	-0.05 ± 0.06	-0.31 ± 0.37	(M)1
3013.5 ± 0.2	959.1 ± 0.1	2054.7	44 ± 1	27/2(+)	$25/2^{+}$	0.83 ± 0.02	-0.01 ± 0.03	-0.06 ± 0.19	(M)1
3066.1 ± 0.2	542.7 ± 0.1	2523.0	46 ± 1	29/2-	27/2+	0.81 ± 0.01	0.04 ± 0.03	0.16 ± 0.12	E1
3093.2 ± 0.4	1038.5 ± 0.3	2054.7	16 ± 3	29/2	$25/2^{+}$	1.24 ± 0.09			${\it Q}$
3107.5 ± 0.2	584.5 ± 0.1	2523.0	21 ± 1	29/2	27/2+	0.66 ± 0.02			\tilde{D}
3108.3 ± 0.4	704.1 ± 0.3	2404.2	11 ± 1	- /	25/2+				
3220.5 ± 0.4	1165.8 ± 0.3	2054.7	6 ± 1		25/2+				
3231.8 ± 0.2	364.5 ± 0.1	2867.2	40 ± 1	$31/2^{+}$	29/2+	0.79 ± 0.02	-0.04 ± 0.03	-0.13 ± 0.10	M1
3236.3 ± 0.2	368.8 ± 0.1	2867.2	79 ± 2	33/2+	29/2+	1.39 ± 0.03	0.03 ± 0.02	0.10 ± 0.06	E2
3241.9 ± 0.2	374.7 ± 0.1	2867.2	15 ± 1	$33/2^{(+)}$	$\frac{29}{2^+}$	1.41 ± 0.04	0.08 ± 0.10	0.26 ± 0.32	(E)2
3254.4 ± 0.2	390.9 ± 0.1	2863.0	18 ± 1	33/2-	31/2+	0.97 ± 0.05	0.08 ± 0.07	0.26 ± 0.23	E1(+M2)
3262.9 ± 0.2	196.6 ± 0.1	3066.1	16 ± 1	33/2	29/2-	1.28 ± 0.04			Q
3264.0 ± 0.2	397.0 ± 0.1	2867.2	22 ± 1	33/2(+)	29/2+	1.20 ± 0.04	0.05 ± 0.06	0.17 ± 0.20	(E)2
3292.0 ± 0.3	1237.2 ± 0.2	2054.7	5 ± 1	/-	25/2+				(-)-
3376.5 ± 0.4	140.2 ± 0.4	3236.3	11 ± 1		$33/2^{+}$				
3416.1 ± 0.3	627.4 ± 0.2	2789.1	11 ± 1		25/2-				
3426.5 ± 0.2	637.3 ± 0.1	2789.1	140 ± 3	$29/2^{-}$	25/2-	1.39 ± 0.02	0.08 ± 0.01	0.35 ± 0.05	E2
3443.2 ± 0.3	211.4 ± 0.2	3231.8	29 ± 1	33/2	$31/2^{+}$	0.72 ± 0.02		****	\overline{D}
3456.2 ± 0.2	192.3 ± 0.1	3264.0	14 ± 1	35/2	$33/2^{(+)}$	0.68 ± 0.05			$\stackrel{D}{D}$
3488.8 ± 0.3	234.3 ± 0.2	3254.4	15 ± 1	35/2	$33/2^{-}$	0.69 ± 0.01			$\stackrel{D}{D}$
3603.8 ± 0.3	1329.9 ± 0.2	2273.6	9 ± 1	22/2	27/2+	2.07 - 0.01			D
3711.9 ± 0.2	844.7 ± 0.1	2867.2	29 ± 1	$33/2^{+}$	$\frac{27}{2}$	1.25 ± 0.05	0.04 ± 0.02	0.22 ± 0.11	E2
3741.7 ± 0.2 3741.7 ± 0.2	315.1 ± 0.1	3426.5	34 ± 1	$31/2^{-}$	$\frac{29}{2}$	0.98 ± 0.04	-0.08 ± 0.02	-0.24 ± 0.11	M1 + E2
3876.6 ± 0.2	450.3 ± 0.1	3426.5	97 ± 2	33/2-	$\frac{29}{2}$	1.33 ± 0.01	0.03 ± 0.03 0.07 ± 0.02	0.24 ± 0.13 0.25 ± 0.07	E2
20,0.0 ± 0.2	491.5 ± 0.2	3443.2	21 ± 1	37/2	33/2	1.35 ± 0.01 1.36 ± 0.07	J.J. I U.U2	0.25 ± 0.07	Q

E_i (keV)	E_{γ} (keV)	E_f (keV)	I_{γ}	J_i^π	J_f^π	$R_{ m ADO}$	$\Delta_{ m pol}$	P	Multipolarity
3979.4 ± 0.3	742.9 ± 0.2	3236.3	23 ± 1	35/2+	33/2+	0.77 ± 0.03	-0.04 ± 0.03	-0.20 ± 0.15	<i>M</i> 1
4146.2 ± 0.2	891.8 ± 0.1	3254.4	4 ± 1		$33/2^{-}$				
4352.3 ± 0.2	475.9 ± 0.1	3876.6	27 ± 1	$35/2^{-}$	$33/2^{-}$	0.77 ± 0.04	-0.06 ± 0.02	-0.22 ± 0.07	M1
4528.2 ± 0.4	175.9 ± 0.3	4352.3	13 ± 1	·	$35/2^{-}$				
4612.0 ± 0.3	735.4 ± 0.2	3876.6	26 ± 1	$35/2^{-}$	$33/2^{-}$	0.90 ± 0.04	-0.05 ± 0.07	-0.25 ± 0.35	M1 + E2
4623.3 ± 0.4	746.7 ± 0.3	3876.6	8 ± 1	·	$33/2^{-}$				
4645.6 ± 0.2	1189.3 ± 0.1	3456.2	11 ± 1	37/2	35/2	0.73 ± 0.04	-0.03 ± 0.07	-0.24 ± 0.56	(M)1
4929.8 ± 0.5	1053.2 ± 0.4	3876.6			$33/2^{-}$				

TABLE I. (Continued.)

the level, as an E2 one herein. Previously [10], the transition was assigned as M1 and the spin-parity of the state (at ≈ 3882 keV, as quoted by Fant *et al.*) as $31/2^-$. Figure 7 represents the spectra of the transition corresponding to the perpendicular and the parallel scattering events and illustrates the dominance of the former that leads to positive value of polarization asymmetry [Eq. (2)] or polarization [Eq. (3)].

(9) The spin-parity of the 4352-keV level has been confirmed to be 35/2⁻ in the present work. The assignment was tentative for the state (at ≈4358 keV, quoted by Fant *et al.*) in the previous studies. The 476-keV transition, deexciting the state, has been identified as M1 in this study and this is different from the E2 assignment by Fant *et al.*

An additional proposition can be put forth on the multipolarity assignment of the 182-keV transition deexciting the 2156-keV state. Since the state is known to be an isomer of $T_{1/2} > 200$ ns [3], the multipolarity of the transition could not be ascertained from its ADO ratio and its polarization asymmetry. These measurements are valid for transitions emitted by a spin-oriented ensemble of nuclei, such as produced in fusion-evaporation reactions, while the aforementioned iso-

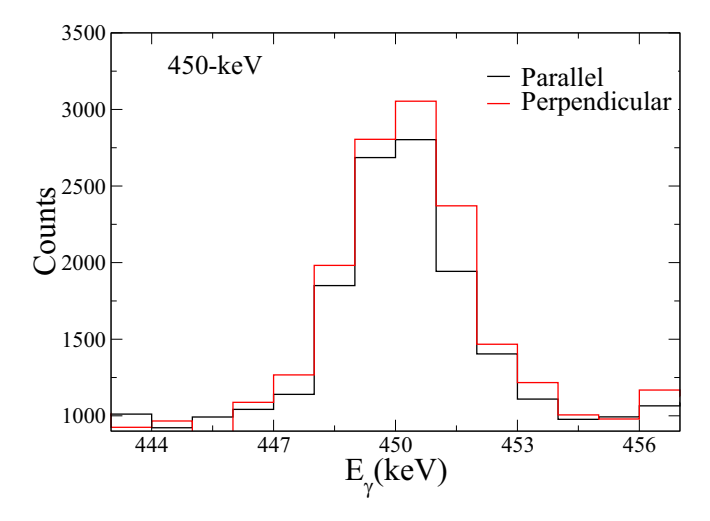


FIG. 7. Spectra of 450-keV transition peak corresponding to the perpendicular and the parallel scattering events in the HPGe clover detectors at 90° .

meric lifetime is sufficient to induce dealignment. If the observed intensity of this 182-keV transition is corrected for electron conversion, using codes such as BrICC [12], it is \approx 60% increased if the transition is an E2 one and \approx 300% enhanced if it is an M1. The latter would result in an unbalanced intensity across the 1975-keV state that is fed by the 182-keV transition and deexcited by the 596-keV one. If the 182-keV transition is thus interpreted to be of E2 nature, the 2156-keV level can be assigned a spin-parity of $25/2^+$. However, since there is no direct experimental evidence for the same, this proposition has not been indicated in the level scheme (Fig. 4) and the assignment has not been included in the table (Table I). Similar perspective can also be assumed for the electromagnetic character of the 234-keV transition that deexcites the 3489-keV state and feeds the level at 3254 keV. It has been identified to be a dipole D following its R_{ADO} value. If it is an E1 transition, the conversion is $\approx 6\%$ while if it is M1, the same is $\approx 100\%$. The latter would offset the intensity balance between the feeding and the decay of the 3254-keV level. This implies that the 234-keV transition is likely to be an E1 and the spin-parity of the 3489-keV state is possibly 35/2⁺. Nevertheless, in the absence of any direct experimental justification, the electromagnetic assignment of the 234-keV transition and the parity assignment of the 35/2 state at 3489 keV have not been included in Table I. The sharp decrease in the relative intensity of the γ -ray transitions across the 2156-keV state is also noteworthy and can be ascribed to the state being an isomer of $T_{1/2} > 200$ ns [3].

Previous studies [3,13] on the Po isotopes had reported a number of isomers therein. Some of these, with half-lives around few ns, have been reexamined in the current study using the centroid shift method [14,15]. In the present implementation of the technique, the time difference between the feeding and the decaying γ -ray transitions of a state is histogrammed alternately by defining one as the start (stop) and the other as stop (start). The timing information of the detections, as recorded by the time-to-digital converter (TDC), have been used for the purpose. The difference between the centroids of the two (aforementioned) distributions is known to be 2τ , τ being the average lifetime of the state. Figure 8 illustrates the time difference spectra between the (i) 788- and 262-keV transitions that respectively feeds and deexcites the 3387-keV state in ²⁰⁴Po [13], also populated in the present experiment, and (ii) 637and 304-keV transitions that respectively feed and deexcite

 $^{^{}a}\Delta J = 0$ transitions exhibit negative (positive) value of polarization for electric (magnetic) nature [16].

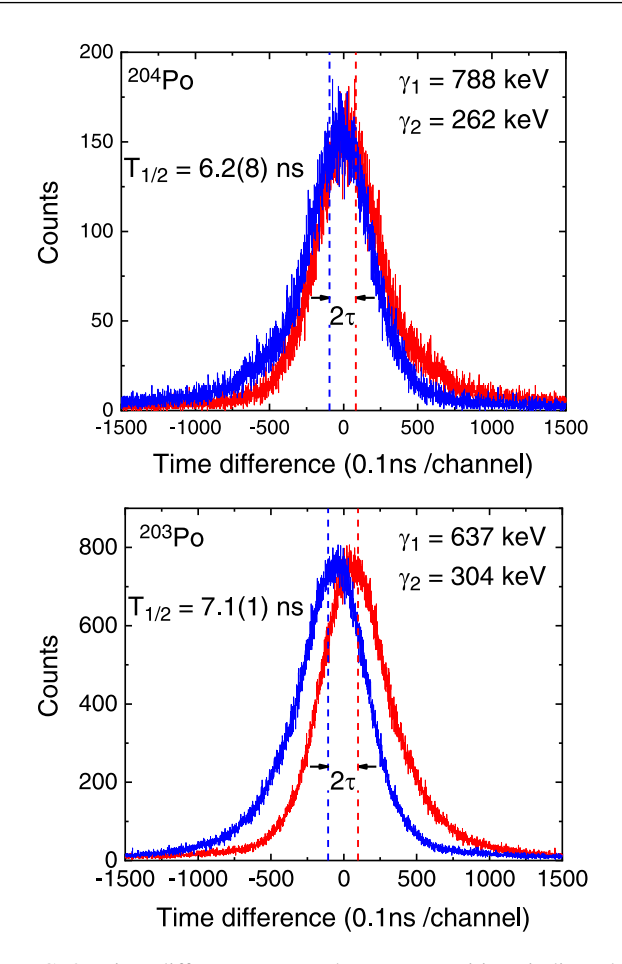


FIG. 8. Time difference spectra between transitions indicated in the inset, for determining isomeric lifetimes. The upper panel corresponds to the state at 3387-keV state in ²⁰⁴Po while the bottom panel is for 2789-keV state in ²⁰³Po. Please refer to the text for details.

the 2789-keV state in ^{203}Po . The half-life of the 3387-keV state in ^{204}Po was determined by Fant et~al.~[13] as 9 ± 3 ns, presumably following an analysis of the time profile of the decaying transition with respect to the rf of the accelerator. The present analysis has resulted in $T_{1/2}=6.2\pm0.8$ ns, which is within the limits of uncertainty on the previous estimate and validates the present analysis. The latter carried out for the 2789-keV state in ^{203}Po yields its $T_{1/2}=7.1\pm0.1$ ns, which is less than the previous value, also reported by Fant et~al.~[3], of 12 ± 2 ns.

The long-lived (isomeric) states are known to effect dealignment in the spin oriented ensemble of nuclei that are produced in fusion-evaporation reactions. The extent of dealignment will presumably depend on the lifetime of the state and the "sufficiently" long-lived ones would de-align the population of nuclei to the extent that the angular distributions of the emitted γ rays therefrom are obliterated. However, a rigid limit on the level lifetime that can benchmark the requisite for significant de-alignment to set in, is still not quoted. As far as the current analysis is concerned, $R_{\rm ADO}$ and polarization values have been determined for the γ rays that directly or indirectly deexcite the isomers in $^{203}{\rm Po}$, with $\tau \approx$ few ns. The resulting assignments have been established to be in overlap

with those in the literature [10]. It follows that the few ns of level lifetimes do not cause considerable de-alignment of the spin oriented population of nuclei that still retain the angular distribution and linear polarization characteristics of the emitted γ rays. It'll be interesting to pursue if the time required for the de-alignment is also dependent on the mass region and if the same lifetimes, that preserve the angular distribution characteristics in these heavy nuclei, will cause de-orientation in the lighter ones.

The experimentally observed level scheme of the ²⁰³Po nucleus has been interpreted through single-particle excitations in the framework of the shell model. The same is detailed in the next section.

IV. DISCUSSIONS

One of the objectives of this endeavor has been to probe the efficacy of the shell model in interpreting the excitation scheme of the nuclei in the $A \approx 200$ region. There have been similar efforts, in recent times, wherein level structures of nuclei around the ^{208}Pb core are calculated in the shell-model framework. Bothe *et al.* [17] have reported such calculations for the isomeric states in ^{203}Tl (Z=81, N=122) while Yadav *et al.* [15] and Madhu *et al.* [14] have used them for deciphering the particle excitations associated with the observed states of $^{215,216}\text{Fr}$ (Z=87, N=128, 129) nuclei. These studies have identified a general overlap, between the experimental and the calculated level energies, of within ≈ 250 keV as reasonable.

Large basis shell-model calculation has been carried out in the present work using the KHH7B [18] Hamiltonian in the model space spanning Z=58-114 and N=100-164. The model space includes proton orbitals $d_{5/2}$, $h_{11/2}$, $d_{3/2}$, and $s_{1/2}$ below Z=82 and the $h_{9/2}$, $f_{7/2}$, and $i_{13/2}$ above; the neutron orbitals are $i_{13/2}$, $p_{3/2}$, $f_{5/2}$, and $p_{1/2}$ below N=126 and the $g_{9/2}$, $i_{11/2}$, and $j_{15/2}$ above. Proton excitations across Z=82 closure and neutron excitations across the closure at N=126 have not been allowed in the calculations. The matrix diagonalization has been carried out using the OXBASH [19] code. The comparison between the calculated and the experimental level energies is illustrated in Figs. 9 and 10. The dominant particle configurations along with the energy values of the states are recorded in Table II.

The calculated energies of the negative-parity states with spin $<\!29/2$ are excellent overlap with their experimental values, even within $\approx\!100$ keV for some of them. The $25/2^-$ level is an exception for which the theoretical and the measured level energies differ by $\approx\!800$ keV. The dominant particle configurations associated with these states negative-parity states have been calculated to be $\pi(h_{9/2}^2) \otimes \nu(f_{5/2}^2 p_{3/2}^2 i_{13/2}^{14})$. The negative-parity states at higher spins, $\geqslant\!31/2$, are poorly represented in the calculations wherein their energies are deviant by as much as 500 keV to 1 MeV with respect to the experimental values. The energy of the calculated yrast $33/2^-$ state, however, reasonably overlaps with the measured energy within $\approx\!250$ keV. The most probable particle configurations for the negative-parity states at higher spins correspond to $\pi(h_{9/2}^1 i_{13/2}^1) \otimes \nu(f_{5/2}^2 p_{3/2}^4 i_{13/2}^{13/2})$.

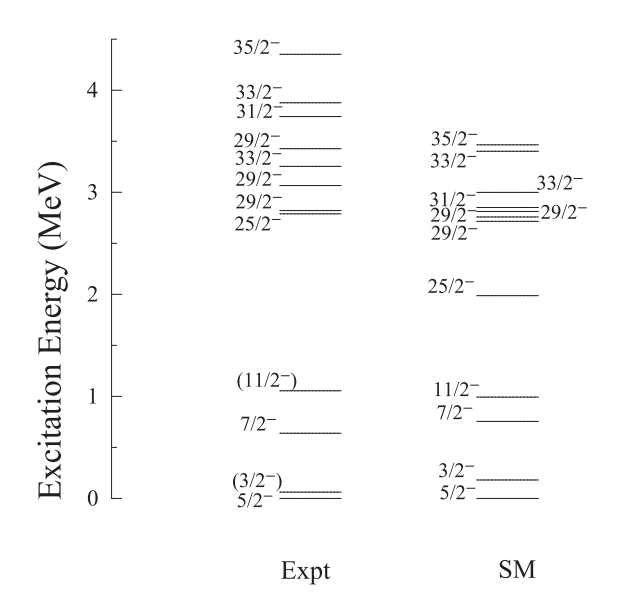


FIG. 9. Comparison between the calculated and the experimental level energies of the negative-parity states in ²⁰³Po.

However, those of the yrare $33/2^-$ and the $35/2^-$ are different $[\pi(h_{9/2}^2) \otimes \nu(f_{5/2}^3 p_{3/2}^4 i_{13/2}^{12})]$ but, as indicated by the widely deviant calculated energies vis à vis the experimental ones, these configurations do not appropriately represent the relevant states, similar to the other high spin levels of odd parity. The calculated level energies for most of the positive-parity states with spin <27/2 are in excellent overlap, within or around 100 keV, with their experimental values. The yrare $17/2^+$ state is an exception for which the calculated and the experimental energies differ by ≈500 keV. However, it is noteworthy that the spin-parity assignment of the 1379-keV state as second $17/2^+$ was by Fant *et al.* [3] and is tentative. This could not be confirmed in the present study. If the parity assignment of the state is changed, it would be the yrast (and only observed) 17/2⁻ level with calculated energy of 1214 keV that is in reasonable overlap with the experimental value. Note that, in such a scenario, the 737-keV $(17/2^- \rightarrow 13/2^+)$ and 596-keV $(21/2^+ \rightarrow 17/2^-)$ transitions would be M2 ones and, according to the Weisskopf estimate, would translate into lifetimes of few ns for the states they deexcite. These lifetimes are much less than the γ - γ coincidence window (200 ns) of the experiment and, thus, will not impact the observed intensity of the transitions. The yrast and the yrare 23/2⁺ state respectively exhibit differences of \approx 500 keV and \approx 200 keV between their theoretical and measured values. While the latter can still be perceived as a reasonable overlap, a deviation of the calculated energy by \approx 500 keV with respect to the experimental one indicates an aberrant representation of the state in the framework of the shell-model calculations. It is also noteworthy that the yrast 23/2+ state is calculated to be of substantially mixed configurations, compared with the other states of the nucleus, and the numerically dominant partition is only of 13% probability. As far as the positive-parity states of spin $\geq 29/2$ are concerned, the overlap of experimental and calculated energies is of considerable variance. While they excellently agree for the yrast $31/2^+$, the yrare and the third $33/2^+$ levels, within ≈ 100 keV, the difference is $\approx 250-450$ keV for the $29/2^+$ and the yrast $31/2^+$ and $33/2^+$. It is still higher, ≈ 700 keV, for $35/2^+$. However, as discussed in the preceding section, if the state at 3489 keV is indeed $35/2^+$, it would be the yrast one and the level energy will better agree with its calculated value. The deviations, at the highest excitations observed in the nucleus, can be ascribed to the limitations of the model calculations in representing the associated multiparticle configurations based on the high-j orbitals (that characterize the relevant model space). Most of the positive-parity states have been calculated to be of dominant configuration $\pi(h_{9/2}^2) \otimes \nu(f_{5/2}^{2-4}p_{3/2}^{2-4}i_{13/2}^{13})$. The exceptions are the yrare 25/2+ state, for which the calculated dominant configuration is $\pi(h_{9/2}^1 i_{13/2}^1) \otimes$ $\nu(f_{5/2}^3p_{3/2}^2i_{13/2}^{14})$, and the yrast $27/2^+$ state, for which the most probable configuration is $\pi(h_{9/2}^1 i_{13/2}^1) \otimes \nu(f_{5/2}^1 p_{3/2}^4 i_{13/2}^{14})$. It is noteworthy that the calculated and the experimental energies of these states agree within ≈50 keV that presumably vindicates the interpretation of their underlying excitations.

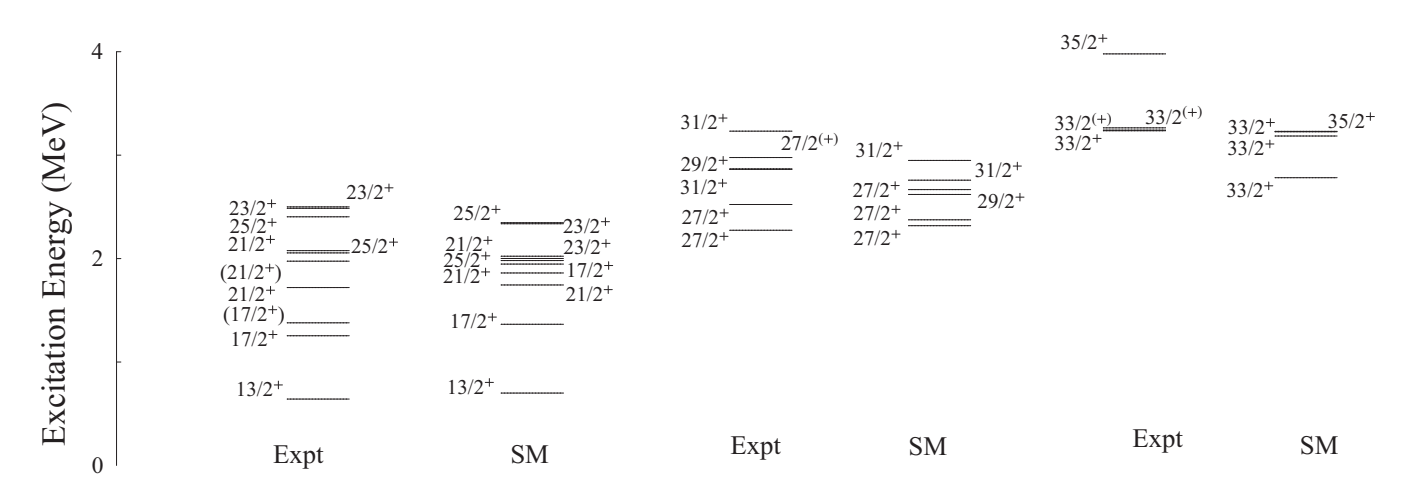


FIG. 10. Comparison between the calculated and the experimental level energies of the positive-parity states in ²⁰³Po.

TABLE II. Main partitions of wave functions of the positive- and negative-parity states in 203 Po for KHH7B interaction. The probability of the most dominant configuration is expressed in % of the total wave function of the state.

Level energy									
Expt.	SM	J^{π}	Probability	Proton	Neutron				
Negative parity									
0	0	$5/2^{-}$	29.33	$h_{9/2}^2 f_{7/2}^0 i_{13/2}^0$	$f_{5/2}^3 p_{3/2}^2 p_{1/2}^0 i_{13/2}^{14}$				
62	181	$(3/2^{-})$	39.21	$h_{9/2}^2 f_{7/2}^0 i_{13/2}^0$	$f_{5/2}^2 p_{3/2}^3 p_{1/2}^0 i_{13/2}^{14}$				
639	755	$7/2^{-}$	19.96	$h_{9/2}^2 f_{7/2}^0 i_{13/2}^0$	$f_{5/2}^2 p_{3/2}^3 p_{1/2}^0 i_{13/2}^{14}$				
1055	993	$(11/2^{-})$	37.64	$h_{9/2}^2 f_{7/2}^0 i_{13/2}^0$	$f_{5/2}^2 p_{3/2}^3 p_{1/2}^0 i_{13/2}^{14}$				
2789	1987	$25/2^{-}$	39.78	$h_{9/2}^2 f_{7/2}^0 i_{13/2}^0$	$f_{5/2}^3 p_{3/2}^2 p_{1/2}^0 i_{13/2}^{14}$				
2821	2715	$29/2^{-}$	70.95	$h_{9/2}^2 f_{7/2}^0 i_{13/2}^0$	$f_{5/2}^3 p_{3/2}^2 p_{1/2}^0 i_{13/2}^{14}$				
3066	2758	$29/2^{-}$	31.65	$h_{9/2}^2 f_{7/2}^0 i_{13/2}^0$	$f_{5/2}^3 p_{3/2}^4 p_{1/2}^0 i_{13/2}^{12}$				
3254	2999	$33/2^{-}$	26.06	$h_{9/2}^1 f_{7/2}^0 i_{13/2}^1$	$f_{5/2}^2 p_{3/2}^4 p_{1/2}^0 i_{13/2}^{13}$				
3427	2812	$29/2^{-}$	24.93	$h_{9/2}^1 f_{7/2}^0 i_{13/2}^1$	$f_{5/2}^2 p_{3/2}^4 p_{1/2}^0 i_{13/2}^{13}$				
3742	2851	$31/2^{-}$	25.53	$h_{9/2}^1 f_{7/2}^0 i_{13/2}^1$	$f_{5/2}^2 p_{3/2}^4 p_{1/2}^0 i_{13/2}^{13}$				
3877	3402	$33/2^{-}$	42.34	$h_{9/2}^2 f_{7/2}^0 i_{13/2}^0$	$f_{5/2}^3 p_{3/2}^4 p_{1/2}^0 i_{13/2}^{12}$				
4352	3465	$35/2^{-}$	24.51	$h_{9/2}^1 f_{7/2}^0 i_{13/2}^1$	$f_{5/2}^2 p_{3/2}^4 p_{1/2}^0 i_{13/2}^{13}$				
4612	3671	$35/2^{-}$	29.32	$h_{9/2}^2 f_{7/2}^0 i_{13/2}^0$	$f_{5/2}^3 p_{3/2}^4 p_{1/2}^0 i_{13/2}^{12}$				
Positive parity									
642	700	$13/2^{+}$	24.13	$h_{9/2}^2 f_{7/2}^0 i_{13/2}^0$	$f_{5/2}^2 p_{3/2}^4 p_{1/2}^0 i_{13/2}^{13}$				
1254	1365	$17/2^{+}$	28.43	$h_{9/2}^2 f_{7/2}^0 i_{13/2}^0$	$f_{5/2}^2 p_{3/2}^4 p_{1/2}^0 i_{13/2}^{13}$				
1379	1861	$(17/2^+)$	23.95	$h_{9/2}^2 f_{7/2}^0 i_{13/2}^0$	$f_{5/2}^2 p_{3/2}^4 p_{1/2}^0 i_{13/2}^{13}$				
1720	1745	$21/2^{+}$	23.00	$h_{9/2}^2 f_{7/2}^0 i_{13/2}^0$	$f_{5/2}^2 p_{3/2}^4 p_{1/2}^0 i_{13/2}^{13}$				
1975	1947	$(21/2^+)$	30.87	$h_{9/2}^2 f_{7/2}^0 i_{13/2}^0$	$f_{5/2}^4 p_{3/2}^2 p_{1/2}^0 i_{13/2}^{13}$				
2055	1981	$25/2^{+}$	32.32	$h_{9/2}^2 f_{7/2}^0 i_{13/2}^0$	$f_{5/2}^2 p_{3/2}^4 p_{1/2}^0 i_{13/2}^{13}$				
2077	2023	$21/2^{+}$	27.80	$h_{9/2}^2 f_{7/2}^0 i_{13/2}^0$	$f_{5/2}^2 p_{3/2}^4 p_{1/2}^0 i_{13/2}^{13}$				
2404	2347	$25/2^{+}$	35.75	$h_{9/2}^1 f_{7/2}^0 i_{13/2}^1$	$f_{5/2}^3 p_{3/2}^2 p_{1/2}^0 i_{13/2}^{14}$				
2486	2001	$23/2^{+}$	29.66	$h_{9/2}^2 f_{7/2}^0 i_{13/2}^0$	$f_{5/2}^2 p_{3/2}^4 p_{1/2}^0 i_{13/2}^{13}$				
2500	2337	$23/2^{+}$	26.50	$h_{9/2}^1 f_{7/2}^0 i_{13/2}^1$	$f_{5/2}^3 p_{3/2}^2 p_{1/2}^0 i_{13/2}^{14}$				
2274	2318	$27/2^{+}$	22.42	$h_{9/2}^1 f_{7/2}^0 i_{13/2}^1$	$f_{5/2}^1 p_{3/2}^4 p_{1/2}^0 i_{13/2}^{14}$				
2523	2375	$27/2^{+}$	26.22	$h_{9/2}^2 f_{7/2}^0 i_{13/2}^0$	$f_{5/2}^2 p_{3/2}^4 p_{1/2}^0 i_{13/2}^{13}$				
2977	2667	$27/2^{(+)}$	31.61	$h_{9/2}^2 f_{7/2}^0 i_{13/2}^0$	$f_{5/2}^3 p_{3/2}^3 p_{1/2}^0 i_{13/2}^{13}$				
2867	2620	$29/2^{+}$	35.78	$h_{9/2}^2 f_{7/2}^0 i_{13/2}^0$	$f_{5/2}^2 p_{3/2}^4 p_{1/2}^0 i_{13/2}^{13}$				
2863	2758	$31/2^{+}$	53.28	$h_{9/2}^2 f_{7/2}^0 i_{13/2}^0$	$f_{5/2}^2 p_{3/2}^4 p_{1/2}^0 i_{13/2}^{13}$				
3232	2949	$31/2^{+}$	32.75	$h_{9/2}^2 f_{7/2}^0 i_{13/2}^0$	$f_{5/2}^4 p_{3/2}^2 p_{1/2}^0 i_{13/2}^{13}$				
3236	2782	$33/2^{+}$	52.68	$h_{9/2}^2 f_{7/2}^0 i_{13/2}^0$	$f_{5/2}^2 p_{3/2}^4 p_{1/2}^0 i_{13/2}^{13}$				
3242	3185	33/2(+)	57.96	$h_{9/2}^2 f_{7/2}^0 i_{13/2}^0$	$f_{5/2}^3 p_{3/2}^3 p_{1/2}^0 i_{13/2}^{13}$				
3264	3226	33/2(+)	30.14	$h_{9/2}^2 f_{7/2}^0 i_{13/2}^0$	$f_{5/2}^2 p_{3/2}^4 p_{1/2}^0 i_{13/2}^{13}$				
3979	3230	35/2+	51.41	$h_{9/2}^2 f_{7/2}^0 i_{13/2}^0$	$f_{5/2}^2 p_{3/2}^4 p_{1/2}^0 i_{13/2}^{13}$				

If the 2156-keV state is assigned a spin-parity of $25/2^+$, as discussed in the previous section, following an E2 assignment for the 182-keV transition (that deexcites the level), the level is then the yrare $25/2^+$ and exhibits a reasonable overlap, within ≈ 200 keV, with the calculated energy (2347 keV). The current yrare $25/2^+$ at 2404 keV is then the third $25/2^+$ state

and its energy is in excellent agreement with the theoretical value of 2383 keV. Once again, since there is no direct experimental evidence to corroborate the spin-parity assignment of the state at 2156 keV, this has not been included in the table.

It may thus be summed up that the observed excitation scheme of the ²⁰³Po nucleus could be satisfactorily interpreted within the framework of the large basis shell-model calculations. The specific deviations might have resulted from the limitations of the Hamiltonian that requires further refinements. The latter is expected to be facilitated by the availability of experimental data through endeavors such as the present study.

V. CONCLUSION

The level structure of the 203 Po nucleus has been probed following its population in 194 Pt(13 C, ^{4}n) reaction at $E_{lab} =$ 74 MeV. The excitation scheme of the nucleus has been established up to \approx 5 MeV and spin \approx 18 \hbar . Twenty-five new γ -ray transitions have been added in the level scheme of the nucleus and spin-parity assignments have been either made or confirmed for a number of states therein. The observed level scheme has been satisfactorily interpreted within the framework of large basis shell-model calculations wherein the excited states of the nucleus have been ascribed to proton excitations in $h_{9/2}$ and $i_{13/2}$ orbitals outside the Z=82 closure and neutron excitations in $f_{5/2}$, $p_{3/2}$, and $i_{13/2}$ orbitals in the N = 126 shell. The overlap between the experimental and the calculated level energies, of ²⁰³Po, upholds the credibility of the shell model in catering to a microscopic description of the excitation scheme even for heavy nuclei in the $A \approx 200$ region and in model space consisting of high-*j* orbitals. Further refinements in the model calculations are envisaged to follow the availability of experimental data.

ACKNOWLEDGMENTS

The authors wish to thank the staff associated with the Pelletron Facility at IUAC, New Delhi, for their help and support during the experiment. We record our deepest gratitude for Prof. Asimananda Goswami and Pradipta Kumar Das, of the Saha Institute of Nuclear Physics (SINP), Kolkata, for their guidance, help, and active contribution in the target preparation. Help and support received from Kausik Basu (UGC-DAE CSR, KC) during the experiment, is appreciated. Help of V. Vishnu Jyothi during the experiment is also acknowledged. P.C.S. acknowledges a research grant from SERB (India), CRG/2019/000556. B.M. acknowledges the support from Department of Science and Technology, Government of India through DST/INSPIRE Fellowship (No. DST/INSPIRE Fellowship/2020/IF200310). U.G. acknowledges the support from US National Science Foundation through Grants No. PHY1762495 and No. PHY2011890. This work is partially supported by the Department of Science and Technology, Government of India (No. IR/S2/PF-03/ 2003-II).

- V. Rahkonen, B. Fant, C. J. Herrlander, K. Honkanen, A. Källberg, and T. Weckström, Nucl. Phys. A 441, 11 (1985).
- [2] T. Weckström, B. Fant, T. Lönnroth, V. Rahkonen, A. Källberg, and C. J. Herrlander, Z. Phys. A: At. Nucl. (1975) 321, 231 (1985).
- [3] B. Fant, T. Weckström, V. Rahkonen, C. J. Herrlander, and A. Källberg, Nucl. Phys. A 453, 77 (1986).
- [4] S. Muralithar, K. Rani, R. Kumar, R. P. Singh, J. J. Das, J. Gehlot, K. S. Golda, A. Jhingan, N. Madhavan, S. Nath *et al.*, Nucl. Instrum. Methods Phys. Res., Sect. A **622**, 281 (2010).
- [5] S. Das, S. Samanta, S. Chatterjee, A. Ghosh, R. Bhattacharjee, R. Raut, S. S. Ghugre, and A. K. Sinha, Proc. DAE Symp. Nucl. Phys. 62, 1066 (2017).
- [6] D. C. Radford, Nucl. Instrum. Methods Phys. Res., Sect. A 361, 297 (1995).
- [7] S. Samanta, S. Das, R. Bhattacharjee, S. Chatterjee, S. S. Ghugre, A. K. Sinha, U. Garg, Neelam, N. Kumar, P. Jones et al., Phys. Rev. C 97, 014319 (2018).
- [8] S. Samanta, S. Das, R. Bhattacharjee, S. Chatterjee, S. S. Ghugre, A. K. Sinha, U. Garg, Neelam, N. Kumar, P. Jones et al., Phys. Rev. C 99, 014315 (2019).
- [9] R. Palit, H. C. Jain, P. K. Joshi, S. Nagaraj, B. V. T. Rao, S. N. Chintalapudi, and S. S. Ghugre, Pramana 54, 347 (2000).

- [10] F. G. Kondev, Nucl. Data Sheets 177, 509 (2021).
- [11] P. B. Semmes, R. A. Braga, R. W. Fink, J. L. Wood, and J. D. Cole, Nucl. Phys. A 464, 381 (1987).
- [12] T. Kibédi, T. W. Burrows, M. B. Trzhaskovskaya, P. M. Davidson, and J. C. W. Nestor, Nucl. Instrum. Methods Phys. Res., Sect. A 589, 202 (2008).
- [13] B. Fant, T. Weckström, and A. Källberg, Phys. Scr. 41, 652 (1990).
- [14] Madhu, K. Yadav, A. Y. Deo, Pragati, P. C. Srivastava, S. K. Tandel, S. G. Wahid, S. Kumar, S. Muralithar, R. P. Singh et al., Phys. Rev. C 105, 034308 (2022).
- [15] K. Yadav, A. Y. Deo, Madhu, Pragati, P. C. Srivastava, S. K. Tandel, S. G. Wahid, S. Kumar, S. Muralithar, R. P. Singh et al., Phys. Rev. C 105, 034307 (2022).
- [16] S. Ali, S. Rajbanshi, A. Bisoi, S. Nag, S. Saha, J. Sethi, T. Trivedi, T. Bhattacharjee, S. Bhattacharyya, S. Chattopadhyay et al., Proc. DAE Symp. Nucl. Phys. 62, 196 (2017).
- [17] V. Bothe, S. K. Tandel, S. G. Wahid, P. C. Srivastava, B. Bhoy, P. Chowdhury, R. V. F. Janssens, F. G. Kondev, M. P. Carpenter, T. Lauritsen *et al.*, Phys. Rev. C 105, 044327 (2022).
- [18] G. H. Herling and T. T. S. Kuo, Nucl. Phys. A 181, 113 (1972).
- [19] B. A. Brown, MSU NSCL Report (2004), p. 1289.